

Free surface flow past topography: A beyond-all-orders approach

CHRISTOPHER J. LUSTRI¹, SCOTT W. MCCUE² and
BENJAMIN J. BINDER³

¹Mathematical Institute, University of Oxford, 24–29 St Giles, Oxford OX1 3LB, UK

²School of Mathematical Sciences, Queensland University of Technology, Brisbane QLD 4101, Australia
email: scott.mccue@qut.edu.au

³School of Mathematical Sciences, University of Adelaide, Adelaide SA 5005, Australia

(Received 3 June 2011; revised 5 January 2012; accepted 9 January 2012;
first published online 9 February 2012)

The problem of steady subcritical free surface flow past a submerged inclined step is considered. The asymptotic limit of small Froude number is treated, with particular emphasis on the effect that changing the angle of the step face has on the surface waves. As demonstrated by Chapman & Vanden-Broeck, (2006) Exponential asymptotics and gravity waves. *J. Fluid Mech.* **567**, 299–326, the divergence of a power series expansion in powers of the square of the Froude number is caused by singularities in the analytic continuation of the free surface; for an inclined step, these singularities may correspond to either the corners or stagnation points of the step, or both, depending on the angle of inclination. Stokes lines emanate from these singularities, and exponentially small waves are switched on at the point the Stokes lines intersect with the free surface. Our results suggest that for a certain range of step angles, two wavetrains are switched on, but the exponentially subdominant one is switched on first, leading to an intermediate wavetrain not previously noted. We extend these ideas to the problem of flow over a submerged bump or trench, again with inclined sides. This time there may be two, three or four active Stokes lines, depending on the inclination angles. We demonstrate how to construct a base topography such that wave contributions from separate Stokes lines are of equal magnitude but opposite phase, thus cancelling out. Our asymptotic results are complemented by numerical solutions to the fully nonlinear equations.

Key words: exponential asymptotics; free surface flows; small-Froude number limit; intermediate waves; trapped-wave solutions

1 Introduction

The problem of steady two-dimensional free surface flow of an ideal fluid past uneven bottom topography has been the subject of much consideration. In order to provide an appropriate background for the problem, we shall refer to the typical channel topography given in Figure 1(a). Upstream the flow is assumed to be uniform, with height H and speed U , while downstream the average height and speed are denoted by D and V , respectively. It is instructive to describe the flow regimes in terms of the upstream and downstream Froude numbers

$$F = \frac{U}{\sqrt{gH}} \quad \text{and} \quad F^* = \frac{V}{\sqrt{gD}}, \quad (1.1)$$

respectively, where g is the acceleration due to gravity.

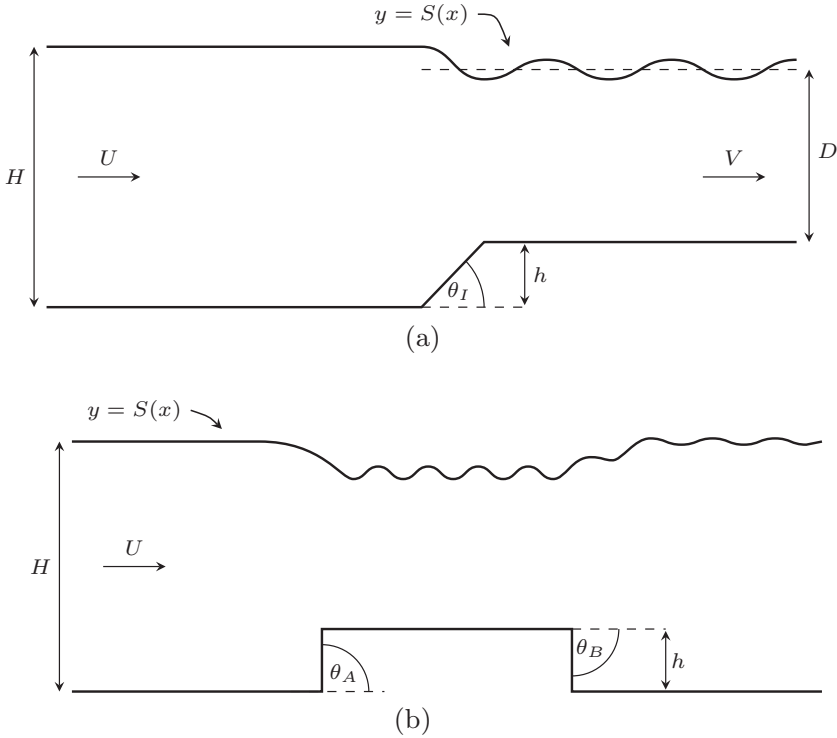


FIGURE 1. Schematics of the two flow configurations considered in this paper. (a) Flow over a submerged step. (b) Flow over a submerged bump.

We are particularly interested in *subcritical flows*, for which these problems are characterised by a train of waves on the downstream free surface. For the linearised problem that applies formally as $\delta = h/H \rightarrow 0$, where h is a measure of the height of the obstruction, this regime has both $F < 1$ and $F^* < 1$. For fully nonlinear flows (with δ finite), this definition is not strictly valid, as more extreme subcritical flows can exist for a small range of Froude numbers $F > 1$ as well as the usual range $F < 1$. (The other two classical regimes, with which we are not concerned, are supercritical and critical flows. Within the linearised framework, the former is defined as having $F > 1$ and $F^* > 1$, while the latter has either $F < 1$ and $F^* > 1$ or $F > 1$ and $F^* < 1$. For a further discussion on the three flow regimes, see [17, 18], for example.)

There are two notable asymptotic limits for the problem of subcritical flow past an uneven topography: one where the Froude number, F , tends to zero, and the other where the height of the obstruction, δ , tends to zero. The former limit is singular, and will be the concern of the bulk of this paper. The latter limit leads itself to the classical linearised formulation, considered by Lamb [25], for example, who studied the flow past a submerged semicircular obstruction. Lamb solves the linear problem exactly, obtaining an explicit formula for shape of the free surface, including the downstream wavetrain. Similar analysis was undertaken by Wehausen & Laitone [41] for the linearised problem of two-dimensional flow past a submerged cylinder. However, as noted by Zhang and Zhu [42], if either stagnation points or singularities occur on the boundary of the flow (at

corners, for example), then for a linear solution to be valid throughout the flow field, the linearisation must take place in an appropriate conformally mapped plane (as in [18,22], for example).

For small Froude numbers $F \ll 1$, care must be taken when treating linear problems valid for $\delta \ll 1$, since a formal power series in δ breaks down in the limit $F \rightarrow 0$ (the correction term in the expansion for $\delta \ll 1$ overtakes the leading order term as $F \rightarrow 0$). Such issues are addressed by Ogilvie [32] and Dagan [13] for the problem of flow past a submerged body, and noted more recently by Zhang & Zhu [42] for flow over topography. As a consequence of this small Froude number nonuniformity, the limits $F \rightarrow 0$ and $\delta \rightarrow 0$ do not commute, and provide a distinguished limit that relates both the Froude number F and the obstruction height δ . The absence of commutivity is not unexpected, since the asymptotic limit $F \rightarrow 0$ is singular, while $\delta \rightarrow 0$ is regular. Additionally, numerical evidence [34,42] suggests that the amplitude of the surface waves becomes exponentially small in the limit $F \rightarrow 0$. A formal power series in F^2 is therefore unable to capture the correct surface wave behaviour of the flow in this limit, as the exponentially small waves take place ‘beyond all orders’ of the power series expansion.

Studies of other two-dimensional free surface problems have demonstrated similar qualitative results in the limit that the Froude number $F \rightarrow 0$. For example, Vanden-Broeck and coauthors treat infinite-depth flows both past a two-dimensional stern [38,39] and due to a submerged line source [38] analytically, and show that for these configurations a power series in the Froude number squared is everywhere divergent. The finite-depth versions of these problems are treated in McCue & Forbes [27] and Mekias & Vanden-Broeck [30], for example, where the main goal was to solve the problems numerically for all Froude numbers; in these cases, numerical results strongly suggest the amplitude of the waves is exponentially small in the Froude number as $F \rightarrow 0$. Other early examples of similar observations are given for flows past submerged bodies and pressure distributions by Dagan [13] and Doctors & Dagan [15]. Note that these are in contrast to certain other configurations, such as flow past a semi-infinite plate [2,26,28,29,31,37], for which solutions with downstream waves do not exist for sufficiently small Froude numbers, and so there is no corresponding small Froude number nonuniformity.

Returning to the subject of free surface flow past a bottom topography, numerical investigations of these problems normally employ a boundary integral method involving complex variable theory, sometimes with the use of conformal mappings. In particular, Forbes & Schwartz [18] treated the flow past a semi-circular obstacle, while King & Bloor [22] solved for the flow over a step. Further early studies are given by [16,23,42,43], for example. Of relevance to the present study, Binder *et al.* [3] recently consider free surface flow over a bump or trench, such as that sketched in Figure 1(b). For subcritical flow, they demonstrate that it is possible to obtain a bump/trench configuration for which the downstream waves past the obstacle are completely eliminated; these are referred to as trapped-wave solutions. Forbes [16] generated trapped-wave solutions for free surface flow over a submerged ellipse, while Binder *et al.* [4] demonstrated that multiple obstacles on the base of the flow could also be used in order to generate trapped surface waves between the two separate obstacles. Similar results have been obtained for obstacles suspended in the flow [19,36] and for flows past pressure distributions [40], for example.

In response to the analytical and numerical evidence noted above, Chapman & Vanden-Broeck [12] have recently constructed an asymptotic framework in which two-dimensional steady free surface flows could be described in the limit $F \rightarrow 0$. These authors employ techniques in exponential asymptotics, developed in [9,33] (and applied to other potential flow problems in [7,8]), that involve applying an asymptotic series expansion in powers of F^2 and capturing the precise factorial/power nature of the divergent tail. After truncating the divergent series optimally, the exponentially small remainder is subsequently analysed using matched asymptotic expansions, providing an expression for the exponentially small surface wave behaviour valid in the limit $F \rightarrow 0$. Chapman & Vanden-Broeck [12] apply this method to the test case of free surface flow over a step, which is illustrated in Figure 1(a) with $\theta_I = \pi/2$. As a result, they demonstrate the existence of a downstream train of exponentially small surface waves with amplitude of order $F^{-2/5}e^{-c/F^2}$, where c is a constant related to the height of the step, as $F \rightarrow 0$. These results were subsequently verified numerically using boundary integral methods. Very recently, Trinh *et al.* [35] applied the techniques developed in [12] to the problem of surface-piercing flow past a semi-infinite stern, resolving many of the issues treated in [38,39].

In the present study, we revisit the problem of free surface flow over a step, and adapt the analysis of Chapman & Vanden-Broeck [12] to allow the step to have an arbitrary angle of inclination, θ_I , as sketched in Figure 1(a). Mathematically this problem is interesting since, as pointed out in [12], Stokes lines are generated by corners with in-fluid angles of greater than $2\pi/3$. Thus for $-\pi/3 < \theta_I < \pi/3$ there are, in general, exponentially small correction terms generated from two active Stokes lines, whereas in the case treated in detail in [12] (that is, $\theta_I = \pi/2$), there is only one such Stokes line. As a result, for $-\pi/3 < \theta_I < \pi/3$ there are two points on the free surface at which exponentially small waves are ‘switched on’. We find that one of the wavetrains has an amplitude of order $F^{-2(3\theta_I-\pi)/(3\theta_I+\pi)}e^{-c/F^2}$ as the Froude number $F \rightarrow 0$, while the other has an amplitude of order $F^{-2(3\theta_I+\pi)/(3\theta_I-\pi)}e^{-1/F^2}$. Downstream, one of these contributions is exponentially subdominant compared to the other (meaning that the smaller of the contributions will be almost impossible to detect in practice); however, for $0 < \theta_I < \pi/3$, there is a finite region, between the points at which the two active Stokes lines intersect the free surface, over which only the smaller of the two contributions is present, leading to an intermediate wavetrain not previously noted for this type of problem. Furthermore, we find that for an infinite number of angles in the range $-\pi/3 < \theta_I < \pi/3$, the amplitude of the subdominant wavetrain vanishes, leaving only the contribution of a single active Stokes line.

To extend these ideas further, we apply the techniques to the problem of flow over a submerged bump or trench, allowing for inclined sides, as in Figure 1(b). In this case there may be two, three or four active Stokes lines, depending on the angles θ_A and θ_B . We find that it is possible to construct the base topography in such a manner that the wave contributions from separate Stokes lines are of equal magnitude, but directly out of phase. As a result, we are able to generate trapped-wave solutions for particular base configurations, supporting the complementary results for the limit that the Froude number $F \rightarrow 1^-$ (with small obstacle height, $\delta \ll 1$) by Binder *et al.* [3] using weakly nonlinear theory.

The layout of the paper is as follows. We begin in Section 2 by formulating the problem of flow over an inclined step using conformal mapping techniques. Subsequently,

in Section 3 we follow the general method outlined by Chapman & Vanden-Broeck [12] for the specific case of flow over an inclined step in order to obtain the exponentially small contribution to the surface behaviour as $F \rightarrow 0$. In Section 4, we present results for this problem and note the possible existence of multiple downstream wavetrains due to the presence of multiple singularities in the flow path. Numerical solutions to the full nonlinear problem are presented to support our findings. The results obtained in Sections 3 and 4 are extended in Section 5 for flow over a submerged bump or trench, particularly noting the possibility of trapped-wave free surface solutions, while the paper concludes in Section 6 with a brief discussion.

2 Formulation for flow over an inclined step

2.1 Governing equations in physical plane

We consider irrotational flow of an incompressible fluid over an inclined step of height h , with the upstream speed given by U , and the upstream channel depth given by H (see Figure 1(a)). We denote the velocity of the fluid as $\mathbf{q}(x, y)$, where $\mathbf{q} = q \cos \theta \mathbf{i} + q \sin \theta \mathbf{j}$, where $q = |\mathbf{q}|$ is the speed of the flow, and θ gives the angle between the streamline and the horizontal at a given point. As the flow is irrotational, we write $\mathbf{q} = \nabla \phi$, where ϕ is the velocity potential. Together with incompressibility $\nabla \cdot \mathbf{q} = 0$, we have Laplace's equation

$$\nabla^2 \phi = 0 \quad (2.1)$$

throughout the flow domain, except at singular points on the boundary.

We scale all velocities by a factor of U and the lengths by a factor of H/π , and use dimensionless equations from here on. The scaled equivalent of the topography in Figure 1(a) is shown in Figure 2(a). In terms of the velocity potential, the problem is now to solve (2.1) subject to

$$\nabla \phi \cdot \hat{\mathbf{n}} = 0 \quad (2.2)$$

on the solid bottom boundary below and the free surface $y = S(x)$ above, where $\hat{\mathbf{n}}$ is a normal vector to these surfaces. Far upstream we have $\phi \sim x$ as $x \rightarrow -\infty$. Finally, we have Bernoulli's equation

$$\frac{1}{2} q^2 + \frac{y}{\pi F^2} = \frac{1}{2} + \frac{1}{F^2} \quad \text{on } y = S(x), \quad (2.3)$$

where F is the upstream Froude number defined in (1.1). To be consistent with Chapman & Vanden-Broeck [12] we shall introduce the parameter $\epsilon = \pi F^2$, but of course the subsequent analysis could as well be applied using F^2 as the small parameter.

2.2 Conformal mapping

As is well known, since the velocity potential ϕ satisfies (2.1), the complex potential $w(z) = \phi + i\psi$ is an analytic function of the complex variable $z = x + iy$ (except at singular points), where ψ is the streamfunction that also satisfies Laplace's equation. We are free to set $\psi = 0$ on the free surface $y = S(x)$, and it therefore follows that $\psi = -\pi$

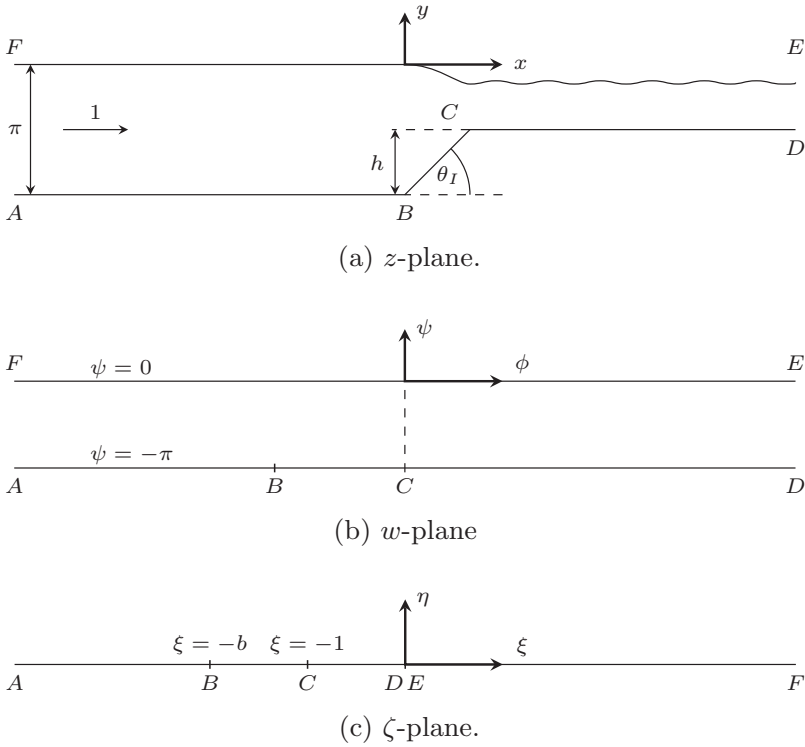


FIGURE 2. Conformal mapping for the dimensionless flow over a submerged step.

on the base of the flow. Fixing these values for ψ has the effect of satisfying the kinematic condition (2.2). We are also free to set a value for ϕ at some point on the base of the channel, and for flow over an inclined step we choose $\phi = 0$ on the top of the step. A schematic of the mapping from the z -plane to the w -plane is shown in Figures 2(a) and (b).

The w -plane is subsequently mapped to the ζ -plane by applying the transformation

$$\zeta = \xi + i\eta = e^{-w}. \tag{2.4}$$

In the ζ -plane, the base of the channel AD maps to the negative real axis ($\eta = 0, \xi < 0$), while the free surface EF maps to the positive real axis ($\eta = 0, \xi > 0$), as indicated in Figure 2(c). The value of the velocity potential ϕ at the point B is unknown *a priori*, and so the location of B in the ζ -plane is also unknown; we label this point $\xi = -b, \eta = 0$. The flow region occupies the upper-half ζ -plane, with the limit $|\zeta| \rightarrow \infty (\eta > 0)$ corresponding to the uniform flow far upstream AF . Note that the mapping (2.4) applies to all channel flows over arbitrary bottom topography, including that treated in Section 5.

It is worth noting that we could have just as easily mapped the uniform flow far upstream AF to the origin $\zeta = 0$ via $\zeta = e^w$, and consequently mapped ED to the far field $\zeta = \infty$; indeed, Hocking & Forbes [20] recommend such an approach, as it avoids mapping a limiting flow region with period waves to a single point (leading to what Hocking & Forbes refer to as an ‘unpleasant’ type of singularity). However, we wish to follow [12] as closely as possible, and so adopt (2.4) as they did. Further, many authors

apply conformal transformations that map periodic waves to a single point for flow over uneven topography, apparently with considerable success (see [3, 22, 43], for example).

2.3 Boundary integral approach

The complex velocity $dw/dz = qe^{-i\theta}$ is an analytic function of z and, as such, $\ln q - i\theta$ is an analytic function of ζ . We derive an integral equation by applying Cauchy's integral formula to $\ln q - i\theta$, taking the contour to be the part of the real axis $-R < \zeta < R$ together with a semi-circle centred at $\zeta = 0$ with radius R . In the limit $R \rightarrow \infty$, the imaginary part gives

$$\ln q = -\frac{1}{\pi} \int_{-\infty}^{\infty} \frac{\theta(\zeta')}{\zeta' - \zeta} d\zeta', \quad (2.5)$$

where here $q(\zeta)$ and $\theta(\zeta)$ are real quantities on the boundary of the flow domain. The integral in (2.5) is of Cauchy Principal Value type.

For flow over an inclined step, as depicted in Figure 2, the function $\theta(\zeta)$ for $\zeta < 0$ describes the angle of the bottom topography. Since the sloped face of the step maps to $-b \leq \zeta < -1$, we have as an input to the problem

$$\theta(\zeta) = \begin{cases} 0 & \zeta < -b, \\ \theta_I & -b \leq \zeta < -1, \\ 0 & -1 \leq \zeta < 0, \end{cases} \quad (2.6)$$

and thus (2.5) simplifies to

$$\ln q = \frac{\theta_I}{\pi} \ln \left(\frac{\zeta + b}{\zeta + 1} \right) - \frac{1}{\pi} \int_0^{\infty} \frac{\theta(\zeta')}{\zeta' - \zeta} d\zeta', \quad \zeta > 0. \quad (2.7)$$

Equation (2.7) provides one equation relating q and θ on the free surface $\zeta > 0$. It is worth emphasising that solutions to (2.7) identically satisfy Laplace's equation (2.1) and the kinematic condition (2.2).

To close the system we first note that differentiating $\zeta = e^{-w}$ with respect to z gives the inverse transform

$$\frac{dx}{d\zeta} = -\frac{1}{\zeta q} \cos \theta, \quad \frac{dy}{d\zeta} = -\frac{1}{\zeta q} \sin \theta, \quad \zeta > 0. \quad (2.8)$$

Thus differentiating Bernoulli's equation (2.3) with respect to ζ leads to

$$\epsilon q^2 \zeta \frac{dq}{d\zeta} = \sin \theta, \quad \zeta > 0 \quad (2.9)$$

(remembering that we are using the parameter $\epsilon = \pi F^2$, where F is the Froude number). The problem of steady free surface flow over an inclined step therefore consists of the coupled system (2.7) and (2.9) for the unknown functions $q(\zeta)$ and $\theta(\zeta)$ on the free surface $\zeta > 0$, $\eta = 0$. The problem has three parameters: ϵ , which is effectively the Froude number squared; the step angle θ_I ; and $b > 0$, which is a measure of the step height. Given the speed q and angle θ , the shape of the free surface in the physical plane is recovered via

(2.8). Finally, the physical step height h can be found from conservation of mass

$$\lim_{x \rightarrow \infty} \psi(x, h) = - \int_h^\pi q(0) dy,$$

which gives

$$h = \pi \left(1 - \frac{1}{q(0)} \right). \tag{2.10}$$

We emphasise that (2.5) and (2.8)–(2.9) hold for more general flows past a bottom topography, including flow over a bump or trench with inclined sides, as treated in Section 5. The defining characteristics of each flow geometry are provided by the angles of each segment on the bottom, as in (2.6). Thus the first term on the right-hand side of (2.7) is for flow over an inclined step; for other flows this term will change.

2.4 Complexifying the free surface

The two real-valued equations (2.7) and (2.9) hold only on the free surface $\zeta > 0, \eta = 0$. A series expansion for $q(\zeta)$ and $\theta(\zeta)$ in powers of ϵ diverges, this divergence being caused by the presence of singularities in the analytic extension of $q(\zeta)$ and $\theta(\zeta)$ into the complex ζ -plane which (abusing notation somewhat) we refer to as the ζ -plane. Thus, in order to proceed, we analytically continue (2.7) and (2.9) into the upper half ζ -plane, giving

$$\log q - i\theta = \frac{\theta_I}{\pi} \log \left(\frac{\zeta + b}{\zeta + 1} \right) - \frac{1}{\pi} \int_0^\infty \frac{\theta(\zeta')}{\zeta' - \zeta} d\zeta', \tag{2.11}$$

$$\epsilon q^2 \zeta \frac{dq}{d\zeta} = \sin \theta. \tag{2.12}$$

The functions $q(\zeta)$ and $\theta(\zeta)$ that satisfy (2.11)–(2.12) effectively provide a complexified description of the free surface. It will be at the singularities of $q(\zeta)$ and $\theta(\zeta)$ that Stokes lines originate (these will be at $\zeta = -1$ and/or $\zeta = -b$, depending on the angle θ_I) and across the Stokes lines that the exponentially small surface waves will be ‘switched on’. Thus, it is important to treat (2.11)–(2.12) in what follows, instead of the real-valued equations (2.7) and (2.9) (but we note, of course, that (2.11)–(2.12) reduce to (2.7) and (2.9) on the positive ζ -axis).

3 Exponential asymptotics

3.1 Preamble

In order to determine the form of the waves on the free surface, we solve (2.11) and (2.12) asymptotically as $\epsilon \rightarrow 0$. We will apply the method developed in [9, 12], which involves analysing the form of the late-order terms of the (divergent) series expansion (in powers of ϵ ; see (3.1) below) and truncating the series optimally. The error after optimal truncation will be exponentially small in ϵ . The idea is to determine how this exponentially small correction term ‘switches on’ across Stokes lines, and also to calculate where the Stokes lines intersect the free surface. The waves will appear on the surface downstream from this intersection point.

The theory in this section is essentially taken from [12], with the emphasis on the problem of flow over an inclined step (the main ideas carry over to the problem of flow over a bump or trench, treated in Section 5, except that instead of having the important singularities located at $\zeta = -1$ or $-b$, they are at $\zeta = -d, -c, -b$ and $-a$). The new results for flow over an inclined step are provided in Section 4.

3.2 Asymptotic power series expansion

We express the components of the fluid velocity as power series in ϵ :

$$\theta \sim \sum_{n=0}^{\infty} \epsilon^n \theta_n, \quad q \sim \sum_{n=0}^{\infty} \epsilon^n q_n \quad \text{as } \epsilon \rightarrow 0. \tag{3.1}$$

Thus, from (2.11) and (2.12), we have

$$\epsilon \zeta (q_0 + \epsilon q_1 + \dots)^2 \frac{d}{d\zeta} (q_0 + \epsilon q_1 + \dots) = \theta_0 + \epsilon \theta_1 + \dots, \tag{3.2}$$

$$\begin{aligned} \log q_0 + \epsilon \frac{q_1}{q_0} + \dots - i(\theta_0 + \epsilon \theta_1 + \dots) &= \frac{\theta_I}{\pi} \log \left(\frac{\zeta + b}{\zeta + 1} \right) \\ &\quad - \frac{1}{\pi} \int_0^\infty \frac{\theta_0(\zeta') + \epsilon \theta_1(\zeta') + \dots}{\zeta' - \zeta} d\zeta', \end{aligned} \tag{3.3}$$

where the omitted terms are $\mathcal{O}(\epsilon^2)$ or smaller. To leading order we find $\theta_0 \equiv 0$, with the first nonzero terms for q and θ being

$$q_0 = \left(\frac{\zeta + b}{\zeta + 1} \right)^{\theta_I/\pi}, \tag{3.4}$$

$$\theta_1 = -\frac{\theta_I}{\pi} \frac{\zeta(b-1)}{(\zeta+1)(\zeta+b)} \left(\frac{\zeta + b}{\zeta + 1} \right)^{3\theta_I/\pi}. \tag{3.5}$$

Obtaining expressions for the higher-order terms quickly becomes difficult, and in any event is not necessary. A crucial point to note is that the terms $\theta_0(\zeta)$, $q_0(\zeta)$ and $\theta_1(\zeta)$ do not oscillate on the free surface $\zeta > 0$, and so cannot describe wavelike behaviour. Furthermore, since these lower-order terms are waveless, the higher order terms will be as well. The reason that straightforward power series expansion (3.1) does not capture the waves is that the wave amplitude is exponentially small compared to all the terms in (3.1). Thus, the wave behaviour lies ‘beyond all orders’ of the asymptotic power series expansion.

3.3 Late-order terms

In order to truncate (3.1) optimally, we must determine from (3.2)–(3.3) the form of q_n , θ_n as $n \rightarrow \infty$. Following [12], and keeping only terms that will be dominant as $n \rightarrow \infty$, we find

$$q_0^2 \zeta \frac{dq_{n-1}}{d\zeta} + 2q_0 q_1 \zeta \frac{dq_{n-2}}{d\zeta} + \dots + 2q_0 q_{n-1} \zeta \frac{dq_0}{d\zeta} + \dots = \theta_n + \dots, \tag{3.6}$$

$$\frac{q_n}{q_0} - \frac{q_{n-1}q_1}{q_0} + \dots - i\theta_n = -\frac{1}{\pi} \int_0^\infty \frac{\theta_n(\zeta') d\zeta'}{\zeta' - \zeta}, \quad n \geq 3. \tag{3.7}$$

As a means to motivate an appropriate ansatz for q_n and θ_n in the upper ζ -plane (provided in (3.10) below), we note from (3.4) that near $\zeta = -1$ and $\zeta = -b$,

$$q_0 \sim \lambda(\zeta - \zeta_0)^\alpha \quad \text{as } \zeta \rightarrow \zeta_0,$$

where

$$\alpha = -\frac{\theta_I}{\pi}, \quad \lambda = (b - 1)^{\theta_I/\pi}, \quad \text{for } \zeta_0 = -1, \tag{3.8}$$

$$\alpha = \frac{\theta_I}{\pi}, \quad \lambda = (1 - b)^{-\theta_I/\pi}, \quad \text{for } \zeta_0 = -b. \tag{3.9}$$

Using (3.6)–(3.7), we are able to obtain the behaviour of each term in the neighbourhood of either $\zeta = -1$ or $-b$, noting that the integral on the right-hand side of (3.7) is subdominant when compared to the left-hand side in the limit that $\zeta \rightarrow -1$ or $-b$, significantly simplifying the expression. We find that

$$q_n \sim i^{n+2} \alpha \mu_n \lambda^{3n+1} (\zeta - \zeta_0)^{n(3\alpha-1)+\alpha}, \quad \theta_n \sim i^{n+1} \alpha \nu_n \lambda^{3n} (\zeta - \zeta_0)^{n(3\alpha-1)}, \tag{3.10}$$

in the neighbourhood of ζ_0 as $n \rightarrow \infty$, where α and λ depend on whether ζ_0 is -1 or $-b$ (through (3.8)–(3.9)), and μ_n and ν_n are polynomials in α of order $n - 1$ with a constant term $(n - 1)!$. Thus, in the neighbourhood of $\zeta = -1$ the late order terms grow in the familiar factorial/power rate when $\theta_I > -\pi/3$ (forcing $3\alpha - 1 < 0$), while in the neighbourhood of $\zeta = -b$ we encounter the same type of divergence when $\theta_I < \pi/3$ (again forcing $3\alpha - 1 < 0$). It follows that for $\theta_I > \pi/3$ there is only one singularity (at $\zeta = -1$), including the special case $\theta_I = \pi/2$ considered in detail by [12]. Similarly, for $\theta_I < -\pi/3$ there is also one singularity (this time at $\zeta = -b$), which includes the case $\theta_I = -\pi/2$ for a step down mentioned in [12]. Interestingly, for $-\pi/3 < \theta_I < \pi/3$ the late order terms diverge near both $\zeta = -1$ and $\zeta = -b$, meaning for this range of step angles there will be two Stokes lines of interest (originating at each of $\zeta = -1$ and $\zeta = -b$), across which waves will be switched on. In general, one of these contributions will be subdominant, meaning that in practice it will not be observed; however, there will be a region on the free surface over which only the subdominant wave train appears (we shall call this an intermediate wavetrain).

While the above argument does not apply away from the singularities at $\zeta = -1$ or b , the asymptotic expansion (3.1) still diverges for any fixed ζ . To obtain the form of the late-order terms q_n and θ_n in the entirety of the upper ζ -plane, Chapman & Vanden-Broeck [12] apply the ansatz

$$\theta_n \sim \frac{\Theta \Gamma(n + \gamma)}{\chi^{n+\gamma}}, \quad q_n \sim \frac{Q \Gamma(n + \gamma)}{\chi^{n+\gamma}} \tag{3.11}$$

as $n \rightarrow \infty$, where χ is forced to be zero at $\zeta = \zeta_0$, with $\zeta_0 = -1$ or $-b$. (For the range $-\pi/3 < \theta_I < \pi/3$, where both singularities exist, the idea is to write θ_n and q_n as a sum of two terms of the form (3.11), with one having $\chi = 0$ at $\zeta = -1$ and the other with $\chi = 0$

at $\zeta = -b$.) By substituting (3.11) into (3.6)-(3.7), Chapman & Vanden-Broeck find that

$$\chi = i \int_{\zeta_0}^{\zeta} \frac{d\zeta'}{\zeta' q_0^3}, \tag{3.12}$$

$$\Theta = -\frac{A}{q_0^3} \exp\left(3i \int_0^{\zeta} \frac{q_1}{\zeta' q_0^4} d\zeta'\right), \quad Q = \frac{A}{q_0^2} \exp\left(3i \int_0^{\zeta} \frac{q_1}{\zeta' q_0^4} d\zeta'\right). \tag{3.13}$$

To obtain these results we must assume the integral on the right-hand side of (3.7) is subdominant as $n \rightarrow \infty$. Arguments in support of this assumption are given recently in Trinh *et al.* [35], and the references therein.

The constants γ and A are found by matching (3.11)–(3.13) with (3.10) near the appropriate singularities $\zeta = -1$ or $-b$, with the result that

$$\gamma = -\frac{6\alpha}{1 - 3\alpha}, \quad A = \frac{\lambda^{6-3\gamma} e^{i\pi\gamma/2}}{2C(1 - 3\alpha)^\gamma} \lim_{n \rightarrow \infty} \frac{\beta_n}{\Gamma(n + \gamma)}, \tag{3.14}$$

where α is related to θ_l through (3.8)–(3.9) (depending on which singularity is appropriate),

$$C = q_0^3(0) \exp\left(-3i \int_0^{\zeta} \frac{1}{\zeta \pi q_0^3} \int_{-\infty}^{\infty} \frac{\theta_1(\xi') d\xi'}{\xi' - \zeta} d\zeta\right)$$

and β_n is given by

$$\beta_0 = 1, \quad \beta_n = \sum_{m=0}^{n-1} \left(m - \frac{2\alpha}{1 - 3\alpha}\right) \beta_m \beta_{n-m-1}.$$

For full details, see [12].

Finally, from Dingle [14], we know that Stokes lines will follow the contour where the successive late-order terms θ_n and q_n have the same phase, which is given by the curve where χ is real and positive. As such, by determining the form of the late-order terms, we have obtained an expression for the path followed by the Stokes line originating from the singularity at $\zeta = \zeta_0$, where $\zeta_0 = -1$ or $-b$. This is significant, as a downstream wavetrain will be switched on at the point where this Stokes line intersects with the free surface. (To be precise, the local condition $3\alpha - 1 < 0$ guarantees a singularity and thus Stokes lines, but the question of whether the Stokes line encounters the free surface is a global issue and depends on the behaviour of q_0 in the complex plane. For the examples treated in this paper the Stokes lines do intersect the free surface.)

3.4 Behaviour in the neighbourhood of Stokes lines

With the form of the late-order terms for q and θ now identified, we truncate (3.1) after N terms and write

$$\theta = \sum_{n=0}^{N-1} \epsilon^n \theta_n + R_N, \quad q = \sum_{n=0}^{N-1} \epsilon^n q_n + S_N, \tag{3.15}$$

where R_N and S_N are the remainder terms. As mentioned above, behaviour that is exponentially small in ϵ as $\epsilon \rightarrow 0$ cannot be demonstrated by the series in (3.15); however,

it is well known that such behaviour is described by R_N and S_N when (3.1) is truncated optimally [1]. The following analysis that shows how the exponentially small wavetrain is made visible is essentially a summary of [12], but with some emphasis on our particular application (by keeping q_0 and q_1 unspecified, the details apply for flows over a more general topology).

By substituting (3.15) into (3.6)–(3.7), we derive a first order differential equation for S_N in the limit $N \rightarrow \infty$ and $\epsilon \rightarrow 0$. The homogeneous version of this equation has a solution $Qe^{-\chi/\epsilon}$, where χ and Q are given by (3.12)–(3.13) (this homogeneous solution is consistent with the ansatz (3.11) for the late order terms), motivating the form

$$S_N = AQe^{-\chi/\epsilon},$$

where the unknown function $A(\zeta; \epsilon)$ is the Stokes multiplier. Optimal truncation gives $N \sim |\chi|/\epsilon$ as $\epsilon \rightarrow 0$, which then provides a differential equation for A in terms of χ and ϵ . By writing $\chi = \rho e^{i\vartheta}$ (here ϑ is not to be confused with the dependent variable θ), matched asymptotic expansions yields

$$A = \frac{\sqrt{2\pi i}}{\epsilon^\gamma} \int_{-\infty}^{\sqrt{\rho}\vartheta/\epsilon} e^{-t^2/2} dt, \tag{3.16}$$

with A clearly varying smoothly and rapidly in the neighbourhood of the point where the Stokes line intersects the free surface, given as $\vartheta = 0$. Finally, matching away from the Stokes line allows us to show that the jump in A across the Stokes line is $2\pi i/\epsilon^\gamma$. The information regarding the remainder R_N is then determined via $R_N \sim -iS_N/q_0$ as $N \rightarrow \infty$. We find that the exponentially small correction terms that are smoothly switched on by the appropriate singularity (either $\zeta = -1$ or $-b$) take the form

$$\frac{2\pi i}{\epsilon^\gamma} \Theta e^{-\chi/\epsilon}, \quad \frac{2\pi i}{\epsilon^\gamma} Q e^{-\chi/\epsilon}, \tag{3.17}$$

respectively, as $\epsilon \rightarrow 0$.

For the above, we have analytically continued (2.7) and (2.9) into the upper half ζ -plane, but an analogous analysis holds if we were to analytically continue into the lower half plane, except that the contribution that switches on as the Stokes line is crossed is the complex conjugate of the terms in (3.17). Taking this contribution into account, and using the notation θ_{exp} to denote the leading order term for the remainder on the free surface $\zeta = \xi$, we have

$$\begin{aligned} \theta_{\text{exp}} &= 2|A\Theta|e^{-\text{Re}(\chi)/\epsilon} \cos\left(\arg \Theta - \frac{\text{Im}(\chi)}{\epsilon}\right) \\ &= \frac{2|A\Lambda|}{q_0^3} e^{-\text{Re}(\chi)/\epsilon} \cos\left(3 \int_0^\xi \frac{q_1}{\xi' q_0^4} d\xi' + \arg \Lambda - \frac{\text{Im}(\chi)}{\epsilon}\right). \end{aligned} \tag{3.18}$$

This expression is clearly oscillatory, and as such demonstrates the existence of the exponentially small free surface waves under investigation. To help compute the term $|A|$

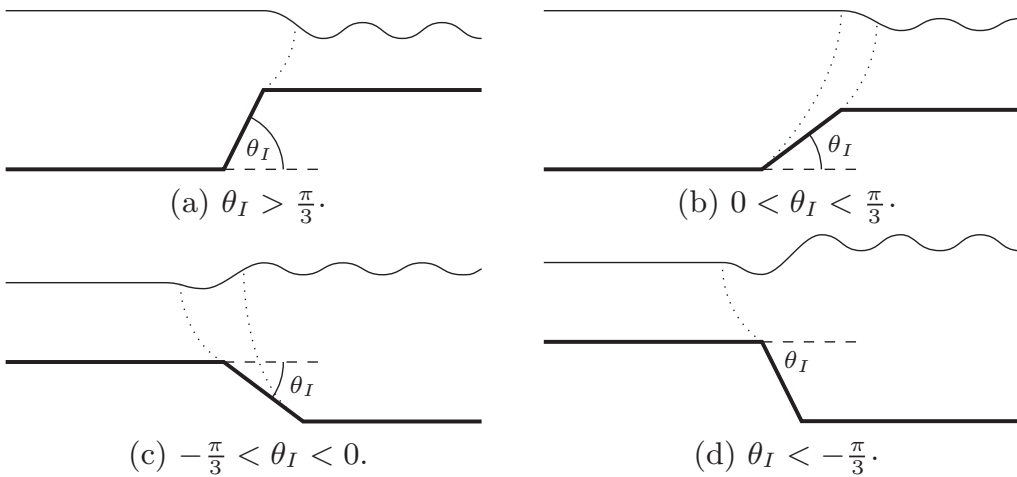


FIGURE 3. Possible configurations for flow over an inclined step, with the Stokes line paths indicated as dotted lines.

in (3.18) we require $|C|$, which works out to be [12]

$$|C| = q_0^3(0) \exp\left(\frac{1}{q_0^3(0)} - 1\right). \quad (3.19)$$

In the following section, we will apply these results to the specific problem of flow over an inclined step.

4 Waves generated over an inclined step

As explained above, for the flow configuration in Figure 2, there are two possible singularities in the ζ -plane, located at $\zeta = -1$ and $\zeta = -b$. As such, there are three different intervals for the step angle θ_I that need to be treated; see Figure 3.

In Figure 3(a), $\theta_I > \pi/3$. For this range of θ_I , the only corner with an in-fluid angle greater than $2\pi/3$ corresponds to $\zeta = -1$. In Figure 3(d), $\theta_I < -\pi/3$. Here, the only corner with an in-fluid angle greater than $2\pi/3$ corresponds to $\zeta = -b$. In both of these configurations, there is only one singularity in the ζ -plane which generates a Stokes line. Therefore, in each of these cases, there is a single downstream wavetrain switched on at the point where the Stokes line intersects the free surface.

In Figures 3(b) and (c), $-\pi/3 < \theta_I < \pi/3$. Here both corners will have in-fluid angles greater than $2\pi/3$, meaning that there are two Stokes lines that intersect the free surface. As such, there are two downstream wavetrains switched on for these configurations.

In order to determine the behaviour of the downstream waves that are switched on in the neighbourhood of the possible Stokes lines, each singularity is considered separately and the contributions added together. Before we proceed, however, we must note some limitations of this approach. First, if the points B and C (see Figure 2) lie too close together (resulting in a small step height), the analysis in the previous section will no longer be valid, as the inner regions near each of the two singularities will overlap. This

case must therefore be approached separately, as explained in Appendix A of [12] for the special case $\theta_I = \pi/2$. Similarly, the above analysis will not be valid in the limit that $\theta_I \rightarrow \pm\pi$, as the base of the channel will lie in the inner region of the singularity, meaning that the configuration must also be approached separately.

4.1 Singularity at $\zeta = -1$

For the singularity at $\zeta = -1$, (3.4) and (3.12) combine to give

$$\chi = i \int_{-1}^{\zeta} \left(\frac{\zeta' + 1}{\zeta' + b} \right)^{3\theta_I/\pi} \frac{d\zeta'}{\zeta'} \tag{4.1}$$

There is a Stokes line that originates at $\zeta = -1$ (where $\chi = 0$) and follows the path upon which χ is real and positive (i.e. the Stokes line has $\text{Re}(\chi) > 0$ and $\text{Im}(\chi) = 0$). This path intersects the positive ζ -axis (corresponding to the free surface) at a value of ζ that can be determined numerically; it is at this point on the free surface that the wavetrain (3.18) is switched on. The numerical calculation is undertaken by interpreting (4.1) as an integral over a box in the upper half plane (for example, by integrating from $\zeta' = -1$ to $-1 + i$, then $\zeta' = -1 + i$ to $1 + i$, then $\zeta' = 1 + i$ to 1) and evaluating the resulting integrals using MATLAB's 'quad' function, which uses an adaptive Simpson quadrature. On the other hand, by indenting the contour clockwise around the pole at $\zeta = 0$, the real part of χ for any $\zeta > 0$ is given exactly by

$$\text{Re}(\chi) = -\pi i \text{Res}_{\zeta=0} \left\{ \frac{i}{\zeta} \left(\frac{\zeta + 1}{\zeta + b} \right)^{3\theta_I/\pi} \right\} = \pi \left(\frac{1}{b} \right)^{3\theta_I/\pi} .$$

Using the general expression for the exponential, given in (3.18), with the components (3.4), (3.8) and (3.14), we find

$$\begin{aligned} \theta_{\text{exp},-1} = & |A| \left(\frac{\pi(b-1)}{\pi+3\theta_I} \right)^{6\theta_I/(\pi+3\theta_I)} \left(\frac{1}{b} \right)^{3\theta_I/\pi} \exp \left(1 - \left(\frac{1}{b} \right)^{3\theta_I/\pi} - \frac{\pi}{\epsilon} \left(\frac{1}{b} \right)^{3\theta_I/\pi} \right) \\ & \times \lim_{n \rightarrow \infty} \frac{\beta_n}{\Gamma(n+\gamma)} \left(\frac{\zeta+1}{\zeta+b} \right)^{3\theta_I/\pi} \cos \left(3 \int_0^{\zeta} \frac{q_1}{\zeta' q_0^4} d\zeta' + \arg A - \frac{\text{Im}(\chi)}{\epsilon} \right), \end{aligned} \tag{4.2}$$

where, effectively, downstream from the point at which the Stokes line intersects the free surface, $|A| = 2\pi\epsilon^{-6\theta_I/(\pi+3\theta_I)}$ (of course, strictly speaking, this term is smoothly switched on over a very small spatial region via (3.16)).

Given the form of $\theta_{\text{exp},-1}$, we may compute the free surface in the physical plane through

$$\frac{dy}{dx} = \tan \theta \sim \theta,$$

as $\epsilon \rightarrow 0$. As such, integrating $\theta_{\text{exp},-1}$ with respect to x will give the free surface variation caused by the singularity at $\zeta = -1$, denoted $y_{\text{exp},-1}$. Using F instead of ϵ for a moment, the wave amplitude in the far field is therefore of order $F^{-2(3\theta_I-\pi)/(3\theta_I+\pi)} e^{-c/F^2}$ as the Froude number $F \rightarrow 0$, where the constant $c = b^{-3\theta_I/\pi}$. For the case $\theta_I = \pi/2$, this

result agrees with that given in Chapman & Vanden-Broeck [12] (and mentioned in the Introduction).

4.2 Singularity at $\zeta = -b$

A similar analysis holds for the singularity at $\zeta = -b$. In this case the form of χ changes slightly to give

$$\chi = i \int_{-b}^{\zeta} \left(\frac{\zeta' + 1}{\zeta' + b} \right)^{3\theta_1/\pi} \frac{d\zeta'}{\zeta'}. \quad (4.3)$$

Again, the Stokes line originates at $\zeta = -b$ and intersects the ζ -axis at some finite value of ζ ; it is at this point that the wavetrain (3.18) is switched on. Now suppose that ζ is real and positive in (4.3). By integrating from $\zeta' = -b$ to $\zeta' = \zeta > 0$ via a contour that runs from $\zeta' = -b$ to $\zeta' = -\infty$, clockwise around an infinitely large semi-circle, and then from $\zeta' = \infty$ to $\zeta' = \zeta$, we find that

$$\text{Re}(\chi) = \pi.$$

Thus, combining (3.4), (3.9), (3.14) and (3.18), we have

$$\begin{aligned} \theta_{\text{exp},-b} = |A| & \left(\frac{\pi - 3\theta_1}{\pi(1-b)} \right)^{6\theta_1/(\pi-3\theta_1)} \left(\frac{1}{b} \right)^{3\theta_1/\pi} \exp \left(1 - \left(\frac{1}{b} \right)^{3\theta_1/\pi} - \frac{\pi}{\epsilon} \right) \\ & \times \lim_{n \rightarrow \infty} \frac{\beta_n}{\Gamma(n+\gamma)} \left(\frac{\zeta+1}{\zeta+b} \right)^{3\theta_1/\pi} \cos \left(3 \int_0^{\zeta} \frac{q_1}{\zeta' q_0^4} d\zeta' + \arg A - \frac{\text{Im}(\chi)}{\epsilon} \right). \end{aligned} \quad (4.4)$$

In cases, in which $(1-b)^{6\theta_1/(\pi-3\theta_1)}$ is complex, we must take care to include an additional argument in the cosine term. Again, integrating $\theta_{\text{exp},-b}$ with respect to x will give the free surface amplitude, $y_{\text{exp},-b}$. In this case we find the wave amplitude is of order $F^{-2(3\theta_1+\pi)/(3\theta_1-\pi)} e^{-1/F^2}$ as the Froude number $F \rightarrow 0$.

4.3 Flow over an inclined step with one Stokes line

We consider the flow configurations shown in Figures 3(a) and (d). In both of these configurations, there is only one corner with an in-fluid angle greater than $2\pi/3$, and thus only one Stokes line in the ζ -plane originating at the associated singularity. In (a), this corner corresponds to a singularity at $\zeta = -1$. The Stokes line generated at this singularity will follow the path upon which χ , given in (4.1), is real and positive. At the point where this Stokes line intersects the free surface, exponentially small variation in θ , given in (4.2), will be switched on. In (d), however, it is the first corner in the flow path which has an in-fluid angle greater than $2\pi/3$. This angle corresponds to a singularity at $\zeta = -b$, which will generate a Stokes line that follows the curve along which χ , given in (4.3), is real and positive. At the point where this Stokes line intersects the free surface, exponentially small variation in θ , given in (4.4), will be switched on.

Figure 4 shows approximate free surface plots for flow over an inclined step, obtained by computing the early terms $\theta_0 + \epsilon\theta_1$ of the asymptotic expansion (3.1) (or, equivalently, (3.15)) for the position of the free surface, and adding the exponentially small free surface

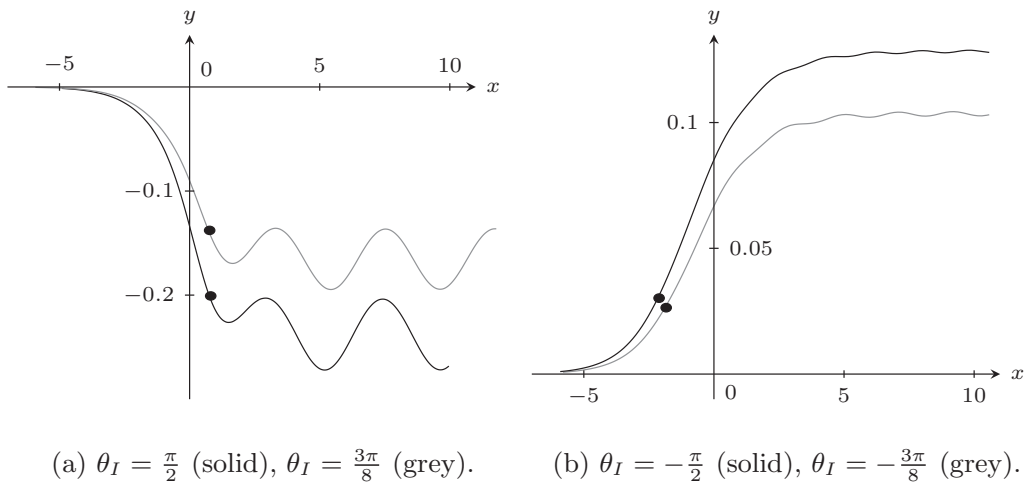


FIGURE 4. Approximate free surface profiles for $b = 2$ and $F = 0.4$, giving $\epsilon = 0.5029$: (a) $\theta_I = \pi/2$ and $3\pi/8$; (b) $\theta_I = -\pi/2$ and $-3\pi/8$. In each flow configuration, there is one Stokes line that intersects the free surface, the intersection point being denoted by a solid circle.

variation (4.2) or (4.4) caused by the singularities in the flow path. For this figure, the angles were selected such that there is only a single corner with an in-fluid angle greater than $2\pi/3$ in the channel, and as such only a single Stokes line that intersects the free surface, originating from this corner.

In Figure 4(a), the angle of inclined step is positive, and it is the second corner in the flow path that generates the Stokes line, while in Figure 4(b) the angle of inclination is negative, and it is the first corner that generates the Stokes line. In each plot, the point at which χ is purely real, and therefore the point at which the Stokes line intersects the free surface, is noted. For the cases in which the wavetrain is generated by the second corner, as in (a), the Stokes line intersects the free surface at a point farther down the flow path than when the wavetrain is generated by the first corner, as in (b).

As a check on the asymptotic results we also compute fully nonlinear solutions, using the numerical scheme of Chapman and Vanden-Broeck [12]. We checked the accuracy of our computations by comparing them with their nonlinear results (Figures 4–7 in [12]) for the special case $\theta = \pi/2$. Shown in Figure 5 is the (logarithm of the) amplitude of the wavetrain in the far field as a function of our small parameter (effectively the Froude number squared) ϵ for two cases: $\theta = \pi/2$ and $3\pi/8$. The solid curve is the asymptotic result, while the solid dots come from our numerical solutions. We see that the agreement is quite reasonable for moderately small values of ϵ , and much better as ϵ decreases.

4.4 Flow over an inclined step with two Stokes lines

We now consider the flow configurations shown in Figures 3(b) and (c). In each of these configurations, there are two angles with an in-fluid angle greater than $2\pi/3$, and as such will generate Stokes lines originating at the two associated singularities in the ζ -plane. Thus, there will be two separate downstream wavetrains in each of these configurations,

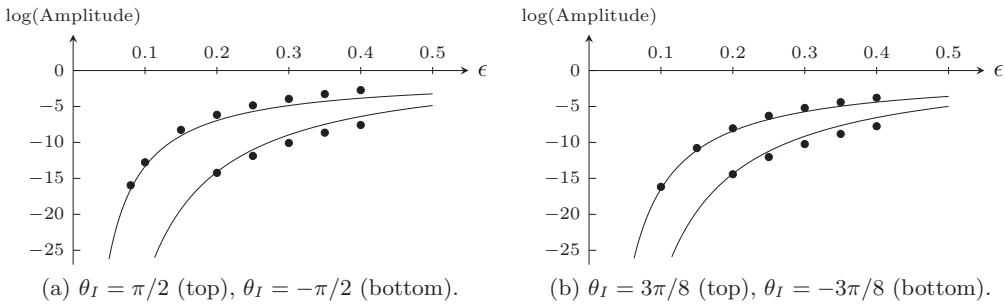


FIGURE 5. Log of far field wave amplitude versus ϵ . The solid curves represent our asymptotic results, while the solid dots represent numerical simulation.

with the exponentially small variation in θ given as

$$\theta_{\text{exp}} = \theta_{\text{exp},-1} + \theta_{\text{exp},-b}.$$

By comparing the magnitude of both terms, it is apparent that the exponentially small variation in θ , for which $\text{Re}(\chi)$ takes the greatest value, will dominate the other exponentially in the limit that $\epsilon \rightarrow 0$. As such, $\theta_{\text{exp},-1}$ will dominate $\theta_{\text{exp},-b}$ when $\theta_I > 0$, while $\theta_{\text{exp},-b}$ will dominate $\theta_{\text{exp},-1}$ for $\theta_I < 0$. (For the case of $\theta_I = 0$, there is no corner in the flow-path, and as such there will be no waves generated.) As a consequence, for any nonzero θ_I for which there are two Stokes lines generated in the flow path, the exponentials generated by one of the Stokes lines will always dominate the other as $\epsilon \rightarrow 0$, precluding the possibility that the two waves could cancel for this geometry (unlike in the analogous problem for capillary waves [11], discussed briefly in Section 6).

Figure 6 shows a comparison of the far field downstream amplitude for the surface waves generated by both singularities over a range of step inclinations. The plot is not symmetric in θ_I , which is consistent with observations by Zhang & Zhu [42], who demonstrated that flow over a semicircular bump and trench of the same size is also not symmetric. We note that the exponential dominance of one wavetrain over the other is apparent, with the waves generated by the singularity at $\zeta = -1$ clearly dominating the waves generated at $\zeta = -b$ for $\theta_I > 0$, while the opposite occurs for $\theta_I < 0$. These results compare relatively well with fully nonlinear results which are shown on the right of the figure.

Interestingly, the amplitude of the subdominant wavetrain appears to be zero for a sequence of isolated angles θ_I . Indeed, we find that β_n converges to zero as $n \rightarrow \infty$ for these values of θ_I , and changes sign as these they are crossed, causing the phase of the surface waves to switch by π . This behaviour is demonstrated in Figure 7, where the appropriate limit is plotted against θ_I . As θ_I decreases, the first few zeros of β_n are at $\theta_I = 0, -0.3668, -0.5389, -0.6414, -0.7085, -0.7565$ and -0.7930 .

For a step with $0 < \theta_I < \pi/3$, the subdominant wavetrain (generated by a Stokes line originating at $\zeta = -b$) will be switched on before the dominant wavetrain (generated by a Stokes line originating at $\zeta = -1$), as shown in Figure 3(b). Therefore, there will be a region of the free surface over which the subdominant waves have been switched on, but

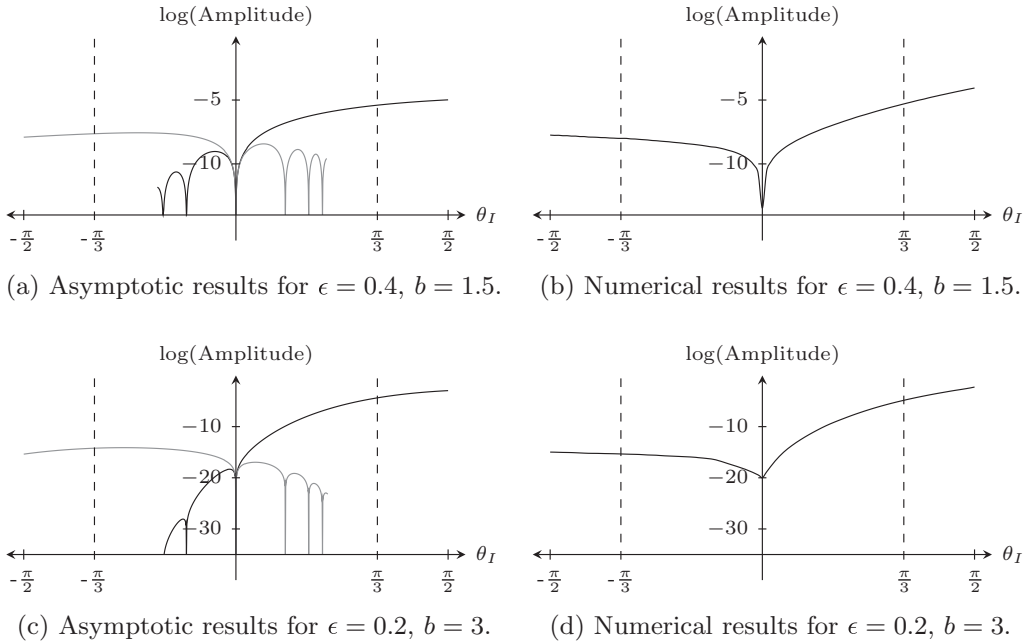


FIGURE 6. Log of far field wave amplitude caused by singularities at $\zeta = -1$ (black) and $\zeta = -b$ (grey), as θ_I is varied, with (a) $\epsilon = 0.2, b = 3$, (c) $\epsilon = 0.4$ and $b = 1.5$. The corresponding numerical results are shown in (b) and (d).

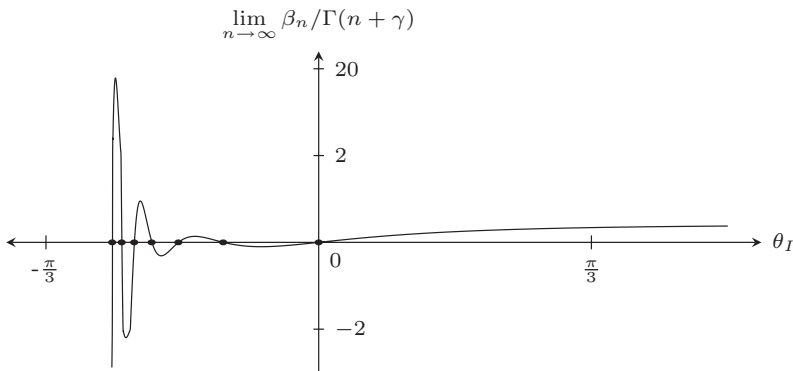


FIGURE 7. This figure demonstrates $\lim_{n \rightarrow \infty} \beta_n / \Gamma(n + \gamma)$ for waves generated by the singularity at $\zeta = -1$ over a range of step inclinations. The points at which the value changes sign, denoted by black dots, occur increasingly rapidly as $\theta_I \rightarrow -\pi/3$.

the dominant waves have not. Our analysis thus predicts the existence of intermediate waves, illustrated in the schematic in Figure 8. Unfortunately, these predicted waves tend to have amplitudes far too small to be detected by our numerical scheme, at least for $\epsilon \ll 1$.

Figure 9 shows approximate free surface plots in the case where both corners have an in-fluid angles greater than $2\pi/3$ in the channel. For the examples $\theta_I = \pm\pi/4$, both

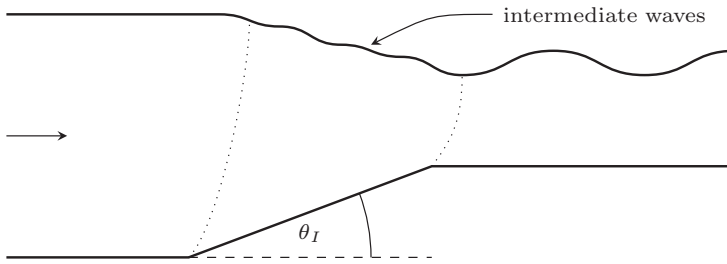
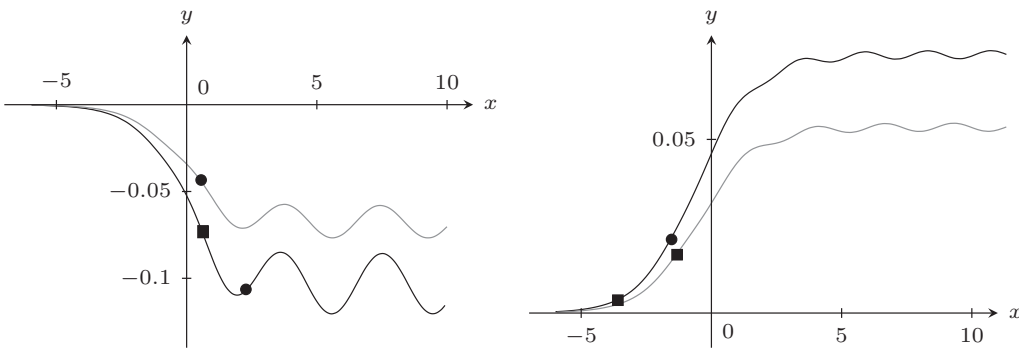


FIGURE 8. Schematic of flow over a submerged step for $0 < \theta_I < \pi/3$, for which our analysis predict the existence of an intermediate wavetrain.



(a) $\theta_I = \frac{\pi}{4}$ (solid), 0.5389 (grey). (b) $\theta_I = -\frac{\pi}{4}$ (solid), -0.5389 (grey).

FIGURE 9. Asymptotic free surface profiles calculated for (a) $\theta_I = \pi/4$ and 0.5389, and (b) $\theta_I = -\pi/4$ and -0.5389. In each case, $b = 2$ and $F = 0.4$, giving $\epsilon = 0.5029$. The Stokes lines that originate at $\zeta = -1$ intersect the free surfaces at points denoted by a circle, while the Stokes lines originating at $\zeta = -b$ intersect at squares.

singularities generate downstream wavetrains, however only the dominant wavetrain is visible. (For $\theta_I = \pi/4$, the dominant wave has amplitude roughly 1.49×10^{-2} , while the subdominant wave has amplitude roughly 3.56×10^{-7} , which explains why we cannot clearly demonstrate both wave trains on a single figure.) For the other two examples $\theta_I = \pm 0.5389$, the angle of inclination was chosen such that $\lim_{n \rightarrow \infty} \beta_n = 0$ and so the amplitude of the subdominant waves (that are switched on at the point on the free surface where the Stokes line is crossed) is zero. Thus the dominant wavetrain is therefore the only nonzero wave contribution that is switched on, despite the in-fluid angle being greater than $2\pi/3$ for both corners.

5 Waves generated over a bump or trench with inclined sides

The ideas outlined in the previous section extend naturally to the problem of flow over a submerged bump or trench with inclined edges. In this case, there are four corners in the flow path, and as such there may be two, three or four Stokes lines present that

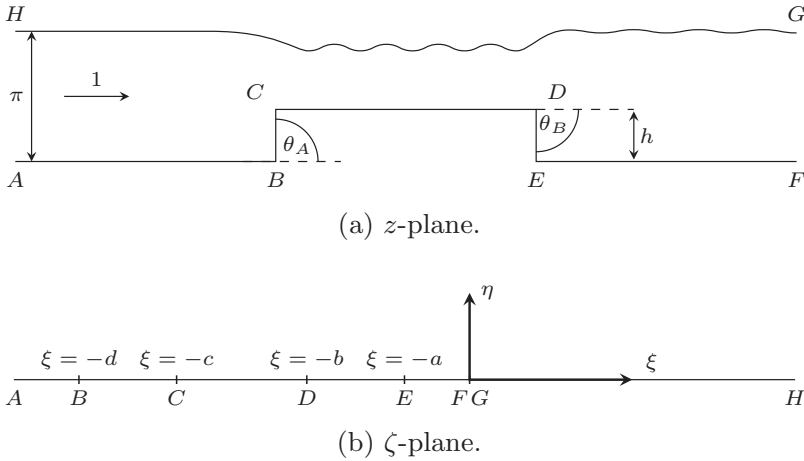


FIGURE 10. Conformal mapping for the dimensionless flow over a submerged bump.

originate at singularities in the ζ -plane. To illustrate the main features, it will be sufficient to consider only cases with two active Stokes lines.

The configuration under consideration is shown in Figure 1(b). If θ_A is positive and θ_B is negative, the channel will contain a bump, while if θ_A is negative and θ_B is positive, the channel will contain a trench. In order to ensure that only two singularities are present in the ζ -plane, we restrict the inclination angles to the range $|\theta_A| > 2\pi/3$ and $|\theta_B| > 2\pi/3$.

The conformal mapping techniques developed in previous sections were applied to this flow configuration, which is demonstrated in Figure 10. Expanding q and θ in power series as in (3.1) in ϵ we find

$$\begin{aligned} \theta_0 &= 0, \\ q_0 &= \left(\frac{\zeta + d}{\zeta + c}\right)^{\theta_A/\pi} \left(\frac{\zeta + a}{\zeta + b}\right)^{\theta_B/\pi}, \\ \theta_1 &= \frac{\zeta}{\pi} \left(\frac{\zeta + d}{\zeta + c}\right)^{3\theta_A/\pi} \left(\frac{\zeta + b}{\zeta + a}\right)^{3\theta_B/\pi} \left(\frac{\theta_A(c - d)}{(\zeta + c)(\zeta + d)} + \frac{\theta_B(a - b)}{(\zeta + a)(\zeta + b)}\right). \end{aligned}$$

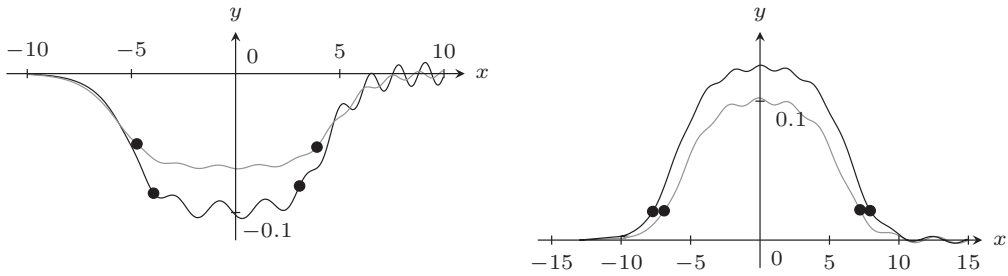
Using identical methods to those presented in the previous section, we find that the downstream wavetrains generated at $\zeta_0 = -a, -b, -c$ and $-d$ take the form

$$\theta_{\text{exp},\zeta_0} = \frac{2|AA_{\zeta_0}|}{q_0^3} \exp\left(-\frac{\text{Re}(\chi_{\zeta_0})}{\epsilon}\right) \cos\left(3 \int_0^\zeta \frac{q_1}{\zeta' q_0^4} d\zeta' + \arg A - \frac{\text{Im}(\chi_{\zeta_0})}{\chi_{\zeta_0}}\right),$$

where

$$\chi_{\zeta_0} = i \int_{\zeta_0}^\zeta \left(\frac{\zeta' + d}{\zeta' + c}\right)^{3\theta_A/\pi} \left(\frac{\zeta' + b}{\zeta' + a}\right)^{3\theta_B/\pi} \frac{d\zeta'}{\zeta'},$$

and A_{ζ_0} and γ_{ζ_0} are determined by (3.14). For flow over a bump or trench, there will always be at least two corners with in-fluid angles of at least $2\pi/3$ in the flow path. As such, the exponentially small variation in θ will be equal to the sum of multiple downstream wavetrains, which switch on at the point where the relevant Stokes line intersects the



(a) $\theta_A = \theta_B = \frac{\pi}{2}$ (solid),
 $\theta_A = \theta_B = \frac{3\pi}{8}$ (grey).
 (b) $\theta_A = \theta_B = -\frac{\pi}{2}$ (solid),
 $\theta_A = \theta_B = -\frac{3\pi}{8}$ (grey).

FIGURE 11. Approximate free surface profiles for (a) a bump with walls of inclination $\pi/2$ and $3\pi/8$ with $\epsilon = 0.2, d = 3000, c = 1500, b = 0.002$ and $a = 0.001$, and (b) a trench with walls of $\pi/2$ and $3\pi/8$ and $\epsilon = 0.5, d = 80, c = 40, b = 0.02$ and $a = 0.01$. In each flow configuration, there are two Stokes lines that intersects the free surface, with the intersection points denoted by circles.

free surface. For simplicity, we will consider only channel configurations which contain two corners that will generate Stokes lines in the ζ -plane, and as such generate two downstream wavetrains. This means that the exponentially small behaviour in θ for flow over a bump will take the form

$$\theta_{\text{exp}} = \theta_{\text{exp},-b} + \theta_{\text{exp},-c},$$

while the exponentially small variation in θ for flow over a trench will take the form

$$\theta_{\text{exp}} = \theta_{\text{exp},-a} + \theta_{\text{exp},-d}.$$

Figure 11(a) shows free surface profiles for flow over a bump with walls having inclinations of $\theta_A = \theta_B = \pi/2$ and $\theta_A = \theta_B = 3\pi/8$, while Figure 11(b) is for flow over a trench with $\theta_A = \theta_B = -\pi/2$ and $\theta_A = \theta_B = -3\pi/8$. In order to contrast with results in the following figure, we note that for these configurations there are clearly waves on the downstream free surface.

If, for a given parameter set, the downstream wavetrains have equal magnitude and are exactly out of phase, the configuration will exhibit trapped wave behaviour, in a similar fashion to that demonstrated in Binder *et al.* [3] using weakly nonlinear theory. In order for the amplitude of the wavetrains to be identical, we require

$$\frac{A_{\zeta_0}}{\epsilon^{\gamma_0}} \exp\left(-\frac{\text{Re}(\chi_{\zeta_0})}{\epsilon}\right) = \frac{A_{\zeta_1}}{\epsilon^{\gamma_1}} \exp\left(-\frac{\text{Re}(\chi_{\zeta_1})}{\epsilon}\right), \tag{5.1}$$

where ζ_0 and ζ_1 are the locations of the two singularities in the ζ -plane. In order for the wavetrains to cancel, we require that

$$-\frac{\text{Im}(\chi_{\zeta_0})}{\epsilon} + \arg A_{\zeta_0} = -\frac{\text{Im}(\chi_{\zeta_1})}{\epsilon} + \arg A_{\zeta_1} + N\pi, \tag{5.2}$$

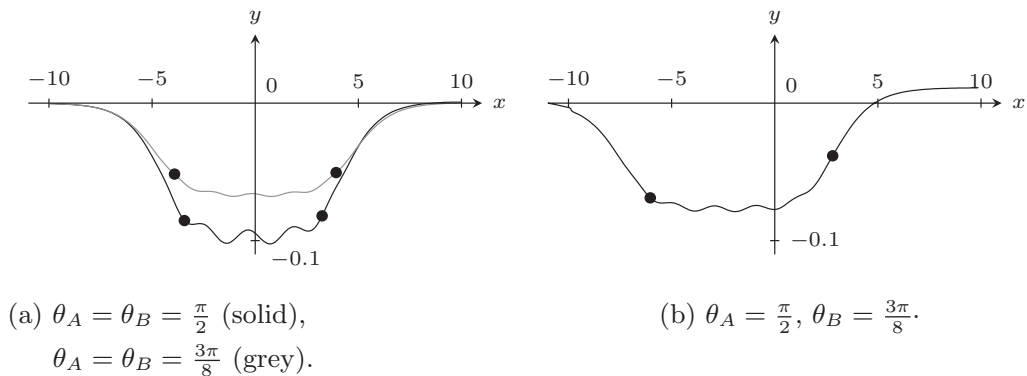


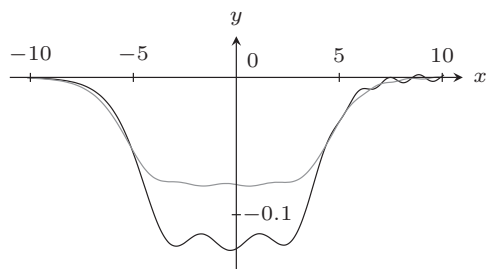
FIGURE 12. Approximate free surface profiles for a bump with walls of inclination (a) $\theta_A = \theta_B = \pi/2$ and $\theta_A = \theta_B = 3\pi/8$ with $\epsilon = 0.2$, and (b) $\theta_A = \pi/2$ and $\theta_B = 3\pi/8$ with $\epsilon = 0.2$.

where N is an odd integer. (If N is chosen to be an even integer, the downstream wavetrains in the resulting configuration will be in phase, and will therefore produce constructive interference between the wavetrains.) We find that if a flow configuration with a bump or trench has one wall with fixed position, and the inclination of each wall is specified, it is generally possible to use these two expressions to determine the position and size of the other wall such that the downstream wavetrains will cancel, thus generating trapped waves over the submerged bump or trench.

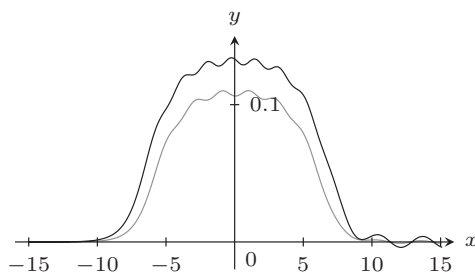
Figure 12 shows approximate free surface profiles for cases in which we have fixed the parameters a and b , and used (5.1) and (5.2) to calculate values for c and d that generate trapped waves. In Figure 12(a), the solid profile is for flow over a bump with sides of inclination $\theta_A = \theta_B = \pi/2$. The values of a and b were set to be 0.001 and 0.002, respectively, as in Figure 11(a). Using (5.1) and (5.2), values for c and d that cause wave cancellation were obtained, giving $c = 750$ and $d = 1500$. Similarly, the grey profile in Figure 12(a) is for $\theta_A = \theta_B = 3\pi/8$. For the same values of a and b , we find that a trapped wave solution exists for $c = 560$ and $d = 1120$. For these examples, the downstream wavetrains are eliminated, and the free surface is therefore flat in the limit $x \rightarrow \infty$.

Figure 12(b) shows that downstream wave cancellation is still possible for bumps and trenches with sides of different inclinations. For flow over an asymmetric bump in Figure 12(b), the first angle of inclination is $\theta_A = \pi/2$ while the second is $\theta_B = 3\pi/8$. Using the prescribed values for a and b of 0.01 and 0.02, as in Figure 11(b), equations (5.1) and (5.2) are used to show that wave cancellation occurs for $c = 24000$ and $d = 51650$ when $\epsilon = 0.2$. It is notable that for this kind of wave cancellation to occur when the walls have the same inclination, the downstream surface height will be identical to the upstream height, but if the walls have different inclination, the downstream height will be different, indicating that the depth of the channel has changed.

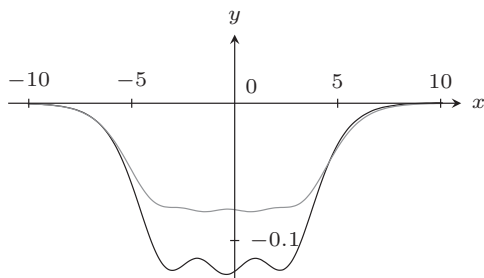
We mention that when the inclination of the walls and the values for a and b are prescribed, there are an infinite number of solutions for c and d that will cause downstream wave cancellation, as adjusting the values of c and d amounts to translating the position of the first wall horizontally until the waves switched on by the two Stokes



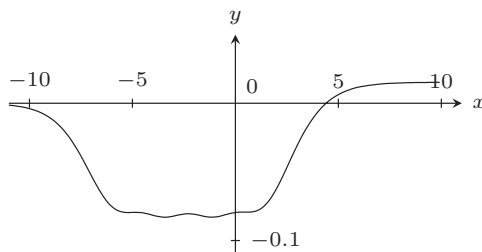
(a) $\theta_A = \theta_B = \frac{\pi}{2}$ (solid),
 $\theta_A = \theta_B = \frac{3\pi}{8}$ (grey).



(b) $\theta_A = \theta_B = -\frac{\pi}{2}$ (solid),
 $\theta_A = \theta_B = -\frac{3\pi}{8}$ (grey).



(c) $\theta_A = \theta_B = \frac{\pi}{2}$ (solid),
 $\theta_A = \theta_B = \frac{3\pi}{8}$ (grey).



(d) $\theta_A = \frac{\pi}{2}, \theta_B = \frac{3\pi}{8}$.

FIGURE 13. Numerically computed free surface profiles. The parameter values for (a) and (b) are the same as Figures 11(a) and (b), respectively. The solid profile in (c) has $c = 1712, d = 3417$; the grey profile in (c) has $c = 1175, d = 2348$; (d) has $c = 19841, d = 40587$. Otherwise, the parameter values in (c) and (d) are the same as Figures 12(a) and (b), respectively.

lines are exactly out of phase. This freedom is reflected in (5.2) by the fact that N may take any odd integer value, and the equation will still hold. Each unique solution corresponds to the presence of a different number of trapped waves in between the Stokes lines.

To support our asymptotic predictions, we present in Figure 13 numerical results computed using the numerical scheme described in Binder *et al.* [3] (which is an extension of that used in Chapman and Vanden-Broeck [12]). The four free surface profiles in Figures 13(a) and (b) are computed using the same parameter values as those in Figures 11(a) and (b). While small in amplitude, the waves on the surface are clearly evident in these plots. The three free surface profiles in Figures 13(c) and (d) are computed using the same values of $\theta_A, \theta_B, \epsilon, a$ and b as the corresponding profiles in Figures 12(a) and (b); however, in order to demonstrate the existence of trapped-wave solutions that are flat far down downstream, we have had to fix the step height and allow the parameters c and d to be found as part of the solution process. Although trapped-wave solutions of this sort were computed numerically in [3] (see Figure 14(a) of that paper), it is worth pointing out that Figure 13(d) demonstrates for the first time that these numerical

solutions exist for flows past a bump with different angles of inclination. We see that numerically computed free surface profiles in Figure 13 compare very well with the asymptotic approximations in Figures 11 and 12. Our main emphasis, however, is to use the numerical results to support our argument that the asymptotic results valid in the limit $\epsilon \rightarrow 0$ can be used to predict and explain qualitative behaviour of free surface flows more generally.

The examples presented above in Figures 11 and 12 should be enough to illustrate the power of using this analysis to describe the variety of flow regimes. By extending these ideas, it is easy to see that for configurations that have three or four corners with an in-fluid angle greater than $2\pi/3$, it is possible that some of the downstream wavetrains could cancel, while others remain. If the two dominant downstream wavetrains cancel, then the resultant flow could only have a single downstream wavetrain, exponentially small compared to the trapped waves. Additionally, if there are four corners with an in-fluid angle greater than $2\pi/3$, it is possible that a, b, c and d may be chosen so that the two dominant wavetrains and the two subdominant wavetrains are of equal amplitude and opposite phase. This leads to both the dominant and subdominant waves being trapped, and therefore the free surface is flat far downstream.

6 Discussion

In this study, we have applied the beyond-all-orders framework developed in [12] to two specific examples of steady two-dimensional free surface flow: flow over an inclined step (Figure 1(a)) and flow over a bump/trench with inclined sides (Figure 1(b)). These examples are characterised by having a different number of Stokes lines, depending on the angles of inclination of the bottom obstruction. We have illustrated a variety of possibilities, including those that exhibit intermediate wavetrains and trapped-wave solutions. Numerical solutions have also been presented to support these scenarios. Note we have not treated the limits that the Froude number $F \rightarrow 0$ with small obstacle height $\delta = h/H \ll F^2$ nor the distinguished limit $F \rightarrow 0$ with $\delta = O(F^2)$, as done in [12] for the step-up problem with $\theta_I = \pi/2$. We expect, however, that the details will follow from [12] closely. Further, we have not given much consideration to the limit $\theta_I \rightarrow \pm\pi/3$, for which there appears to be interesting behaviour not previously encountered.

It is worth contrasting the results in this study to the analogous problem of surface-tension driven flows past a bottom obstruction (ignoring the effects of gravity) in the limit of small surface tension [11]. First, for that problem Stokes lines are generated by all corners of the bottom obstruction, regardless of the in-fluid angle. Thus for the geometry sketched in Figure 1(a), the authors in [11] state there will be exponentially small capillary waves switched on at two points on the free surface for all step angles θ_I (see Figure 9 in [11]). Further, unlike in the present problem, while the phase of the capillary waves will depend on the location of the corners, the amplitude of each wavetrain will be the same. As a consequence, for flow over a step with angle θ_I , it is possible to have the two wave forms cancelling each other in the capillary wave case, but not the gravity-driven wave case.

We close by mentioning some open problems and extensions in this area. First, it should not be difficult to generalise the results in [12] and this paper to hold for

multiple obstructions on the channel bottom, such as those treated numerically in Binder *et al.* [4] (see Figures 8 and 9 of that paper). Presumably it would be possible to describe the switching across Stokes lines for each relevant singularity and thus construct trapped-wave solutions as we have done here.

Second, we note that each example treated in [12] and this paper has had sharp corners, with well-defined singularities in the ζ -plane. While the important point is that these are singularities of the complexified free surface, it happens that they are also singularities on the boundary of the physical flow field. For flows past curved bottom obstructions, such as flow past a semi-circle [18], there are no in-fluid angles greater than $2\pi/3$, but we would still expect there to be exponentially small waves in the limit that the Froude number $F \rightarrow 0$, suggesting there are Stokes lines that intersect the free surface. For these flows the relevant singularities of the complexified free surface may be off the real ξ -axis, although for some geometries it may not be obvious where they are located, or whether they are of the form treated in [12]. There are a plethora of configurations that could be addressed, but once theory for curved solid boundaries is developed, one could solve problems such as flow past a submerged ellipse [16], for example, with a view to explaining trapped waves in the limit $F \rightarrow 0$.

Third, it would be interesting to compute accurate numerical solutions that demonstrate the existence of intermediate waves (illustrated schematically in Figure 8) for Froude numbers that are not small. Success in this regard would further support the argument here and in [12] that qualitative features determined asymptotically in the limit $\epsilon \rightarrow 0$ hold more generally.

Finally, it remains a significant challenge to address time-dependent free surface flows using a beyond all orders approach, especially since the conformal mapping approaches used here for steady flows can no longer be applied. It is worth noting, however, that for the (nonlinear) crystal growth model proposed in [6] and studied using beyond all orders techniques by [9, 24] for example, linear time-dependent generalisations have been treated successfully by [5, 10, 21]. The extent to which all these techniques can be applied to fully nonlinear time-dependent free surface flows is as yet untested.

Acknowledgement

CJL thanks Professor Jonathan Chapman for his guidance and for many fruitful discussions on exponential asymptotics.

References

- [1] BERRY, M. V. (1991) Asymptotics, superasymptotics, hyperasymptotics. In: H. Segur, S. Tanveer & H. Levine (editors), *Asymptotics Beyond All Orders*, Plenum, Amsterdam, pp. 1–14.
- [2] BINDER, B. J. (2010) Steady free-surface flow at the stern of a ship. *Phys. Fluids*, **22**, 012104.
- [3] BINDER, B. J., DIAS, F. & VANDEN-BROECK, J.-M. (2007) Influence of rapid changes in a channel bottom on free-surface flows. *IMA J. Appl. Math.* **73**, 1–20.
- [4] BINDER, B. J., VANDEN-BROECK, J.-M. & DIAS, F. (2005) Forced solitary waves and fronts past submerged obstacles. *Chaos* **15**, 037106.
- [5] BODY, G. L., KING, J. R. & TEW, R. H. (2005) Exponential asymptotics of a fifth-order differential equation. *Euro. J. Appl. Math.* **16**, 647–681.

- [6] BROWER, R. C., KESSLER, D. A., KOPLIK, J. & LEVINE, H. (1983) Geometrical approach to moving-interface dynamics. *Phys. Rev. Lett.* **51**, 1111–1114.
- [7] CHAPMAN, S. J. (1999) On the rôle of Stokes lines in the selection of Saffman-Taylor fingers with small surface tension. *Euro. J. Appl. Math.* **10**, 513–534.
- [8] CHAPMAN, S. J. & KING, J. R. (2003) The selection of Saffman-Taylor fingers by kinetic undercooling. *J. Eng. Math.* **46**, 1–32.
- [9] CHAPMAN, S. J., KING, J. R. & ADAMS, K. L. (1998) Exponential asymptotics and Stokes lines in nonlinear ordinary differential equations. *Proc. Roy. Soc. Lond. A* **454**, 2733–2755.
- [10] CHAPMAN, S. J. & MORTIMER, D. B. (2005) Exponential asymptotics and Stokes lines in a partial differential equation. *Proc. Roy. Soc. Lond. A* **461**, 2385–2421.
- [11] CHAPMAN, S. J. & VANDEN-BROECK, J.-M. (2002) Exponential asymptotics and capillary waves. *SIAM J. Appl. Math.* **62**, 1872–1898.
- [12] CHAPMAN, S. J. & VANDEN-BROECK, J.-M. (2006) Exponential asymptotics and gravity waves. *J. Fluid Mech.* **567**, 299–326.
- [13] DAGAN, G. (1975) Waves and wave resistance of thin bodies moving at low speed: The free-surface nonlinear effect. *J. Fluid Mech.* **69**, 405–416.
- [14] DINGLE, R. B. (1973) *Asymptotic Expansions: Their Derivation and Interpretation*, Academic Press, New York.
- [15] DOCTORS, L. J. & DAGAN, G. (1980) Comparison of nonlinear wave-resistance theories for a two-dimensional pressure distribution. *J. Fluid Mech.* **98**, 647–672.
- [16] FORBES, L. K. (1982) Non-linear, drag-free flow over a submerged semi-elliptical body. *J. Eng. Math.* **16**, 171–180.
- [17] FORBES, L. K. (1988) Critical free-surface flow over a semi-circular obstruction. *J. Eng. Math.* **22**, 3–13.
- [18] FORBES, L. K. & SCHWARTZ, L. W. (1982) Free-surface flow over a semicircular obstruction. *J. Fluid Mech.* **114**, 299–314.
- [19] GAZDAR, A. S. (1973) Generation of waves of small amplitude by an obstacle placed on the bottom of a running stream. *J. Phys. Soc. Japan* **34**, 530.
- [20] HOCKING, G. C. & FORBES, L. K. (1992) Subcritical free-surface flow caused by a line source in a fluid of finite depth. *J. Eng. Math.* **26**, 455–466.
- [21] HOWLS, C. J., LANGMAN, P. J. & OLDE DAALHUIS, A. B. (2004) On the higher-order Stokes phenomenon. *Proc. Roy. Soc. Lond. A* **460**, 2285–2303.
- [22] KING, A. C. & BLOOR, M. I. G. (1987) Free-surface flow over a step. *J. Fluid Mech.* **182**, 193–208.
- [23] KING, A. C. & BLOOR, M. I. G. (1990) Free-surface flow of a stream obstructed by an arbitrary bed topography. *Q. J. Mech. Appl. Math.* **43**, 87–106.
- [24] KRUSKAL, M. D. & SEGUR, H. (1991) Asymptotics beyond all orders in a model of crystal growth. *Stud. Appl. Math.* **36**, 129–181.
- [25] LAMB, H. (1932) *Hydrodynamics*. Cambridge University Press.
- [26] MALEEWONG, M. & GRIMSHAW, R. H. J. (2008) Nonlinear free surface flows past a semi-infinite flat plate in water of finite depth. *Phys. Fluids* **20**, 062102.
- [27] MCCUE, S. W. & FORBES, L. K. (1999) Bow and stern flows with constant vorticity. *J. Fluid Mech.* **399**, 277–300.
- [28] MCCUE, S. W. & FORBES, L. K. (2002) Free-surface flows emerging from beneath a semi-infinite plate with constant vorticity. *J. Fluid Mech.* **461**, 387–407.
- [29] MCCUE, S. W. & STUMP, D. M. (2000) Linear stern waves in finite depth channels. *Q. J. Mech. Appl. Math.* **53**, 629–643.
- [30] MEKIAS, H. & VANDEN-BROECK, J.-M. (1991) Subcritical flow with a stagnation point due to a source beneath a free surface. *Phys. Fluids A* **3**, 2652–2658.
- [31] OGILAT, O., MCCUE, S. W., TURNER, I. W., BELWARD, J. A. & BINDER, B. J. (2011) Minimising wave drag for free surface flow past a two-dimensional stern. *Phys. Fluids* **23**, 072101.

- [32] OGLVIE, T. F. (1968) *Wave Resistance. The Low Speed Limit*. Technical Report, Michigan University, Ann Arbor, MI.
- [33] OLDE DAALHUIS, A. B., CHAPMAN, S. J., KING, J. R., OCKENDON, J. R. & TEW, R. H. (1995) Stokes phenomenon and matched asymptotic expansions. *SIAM J. Appl. Math.* **55**, 1469–1483.
- [34] SCULLEN, D. & TUCK, E. O. (1995) Nonlinear free-surface flow computations for submerged cylinders. *J. Ship Res.* **39**, 185–193.
- [35] TRINH, P. H., CHAPMAN, S. J., & VANDEN-BROECK, J.-M. (2011) Do waveless ships exist? Results for single-cornered hulls. *J. Fluid Mech.* **685**, 413–439.
- [36] TUCK, E. O. & SCULLEN, D. C. (1998) Tandem submerged cylinders each subject to zero drag. *J. Fluid Mech.* **364**, 211–220.
- [37] VANDEN-BROECK, J.-M. (1980) Nonlinear stern waves. *J. Fluid Mech.* **96**, 603–611.
- [38] VANDEN-BROECK, J.-M., SCHWARTZ, L. W. & TUCK, E. O. (1978) Divergent low-Froude-number series expansion of nonlinear free-surface flow problems. *Proc. R. Soc. Lond. A* **361**, 207–224.
- [39] VANDEN-BROECK, J.-M. & TUCK, E. O. (1977) Computation of near-bow or stern flows using series expansion in the Froude number. In: *2nd International Conference on Numerical Ship Hydrodynamics*, University of California, Berkeley, CA.
- [40] VANDEN-BROECK, J.-M. & TUCK, E. O. (1985) Waveless free-surface pressure distributions. *J. Ship Res.* **29**, 151–158.
- [41] WEHAUSEN, J. V. & LAITONE, E. V. (1960) Surface waves. In: *Handbuch der Physik*, Springer, pp. 446–778.
- [42] ZHANG, Y. & ZHU, S. (1996) A comparison of nonlinear waves generated behind a semicircular trench. *Proc. Roy. Soc. Lond. A* **452**, 1563–1584.
- [43] ZHANG, Y. & ZHU, S. (1996) Open channel flow past a bottom obstruction. *J. Eng. Math.* **30**, 487–499.